

Estimation of the $j \times B$ Force Produced by Electron Cyclotron Heating in HSX Plasma^{*)}

Yasuhiro YAMAMOTO, Sadayoshi MURAKAMI, Ching-Chieh CHANG, Santhosh T.A. KUMAR¹⁾, Joseph N. TALMADGE¹⁾, Konstantin LIKIN¹⁾ and David T. ANDERSON¹⁾

Kyoto University, Kyoto 615-8540, Japan

¹⁾*University of Wisconsin-Madison, Madison, Wisconsin 53706, USA*

(Received 10 January 2019 / Accepted 14 April 2019)

The force related to electron cyclotron heating (ECH) is investigated in HSX plasma. Radial diffusion of energetic electrons by ECH produces a canceling return current, which then generates a $j \times B$ force that can play an important role in the toroidal rotation during ECH in HSX plasma. We investigate the energetic electron distribution by ECH by applying GNET code, which can solve the 5D drift kinetic equation for the energetic electron. We evaluate the $j \times B$ force and the collisional force due to the friction of the toroidal drift motion of the energetic electrons. As a result, we obtained a significant force due to the ECH and found that a larger force is obtained in the Mirror configuration than in the quasi-helically symmetric (QHS) one. The magnitude relationship of the force is consistent with that of the experimental flow velocity.

© 2019 The Japan Society of Plasma Science and Nuclear Fusion Research

Keywords: ECH, spontaneous flow, $j \times B$ force, HSX, GNET

DOI: 10.1585/pfr.14.3403105

1. Introduction

Many experiments suggest an important role of toroidal flow in turbulence transport. Recently, spontaneous toroidal flows have been observed in electron cyclotron heating (ECH) plasma in many tokamak and helical devices such as JT-60U, LHD and HSX. It is necessary to clarify the underlying mechanism, and many experimental [1] and theoretical [2] studies have been undertaken to achieve this.

The helically symmetric experiment (HSX) is the first quasi-symmetric stellarator device [3]. There are two typical configurations for HSX. One is Quasi Helically Symmetric (QHS) configuration, which has the helical direction of symmetry in $|B|$. The $(m, n) = (1, 4)$ mode in the Boozer spectrum is dominant in the QHS configuration. The other one is the Mirror configuration, where a set of auxiliary coils makes toroidal mirror terms, the $(0, 4)$ and $(0, 8)$ modes, to the magnetic field spectrum to break the symmetry [4].

Flow measurement experiments have been carried out in HSX by the charge exchange recombination spectroscopy (CXRS) [5]. The QHS configuration leads to a neoclassical viscosity that is smaller than that obtained with the Mirror configuration because of the helical symmetry, so we expected that the toroidal flow velocity in the QHS configuration would be larger than that in the Mirror configuration. However, a smaller toroidal flow has been

observed in the QHS configuration [6, 7], a result that has not been understood well yet.

In this study, we express the torque [N·m] produced by ECH in the form of a force density [N/m³] to ignore the radius effect. We evaluate the direction and strength of the forces generated by ECH using GNET code [8], which can solve a linearized drift kinetic equation in the 5D phase-space, and discuss what makes the difference.

2. Theory and Simulation Model

As mentioned above, to study ECH, we apply GNET code, which can solve the drift kinetic equation in 5-D phase space using the Monte Carlo method. We split the gyrophase averaged electron distribution function, f , into a stationary part, f_{Max} , and an oscillating part by ECH, δf , as $f = f_{\text{Max}} + \delta f$, where we consider that the stationary part is Maxwellian. The drift kinetic equation for δf is given by

$$\begin{aligned} \frac{\partial \delta f}{\partial t} + (\vec{v}_d + \vec{v}_{\parallel}) \cdot \frac{\partial \delta f}{\partial \vec{r}} + \dot{v} \cdot \frac{\partial \delta f}{\partial \vec{v}} - C(\delta f) - L(\delta f) \\ = S^{\text{ql}}(f_{\text{Max}}), \end{aligned} \quad (1)$$

where \vec{v}_{\parallel} and \vec{v}_d are the velocity parallel to the magnetic field and the drift velocity, respectively. Also, $C(\delta f)$, $L(\delta f)$ and $S^{\text{ql}}(f_{\text{Max}})$ are the collision operator, the orbit loss term, and the quasi-linear diffusion operator as the source term for the absorption of ECH, respectively.

The ECH driving term is described by the quasi-linear diffusion theory. We consider that interaction between the EC waves and the particles are so long that the plasma can reach the steady state. Here we have ignored the quasi-

author's e-mail: yamamoto_y@p-grp.nucleng.kyoto-u.ac.jp

*) This article is based on the presentation at the 27th International Toki Conference (ITC27) & the 13th Asia Pacific Plasma Theory Conference (APPTC2018).

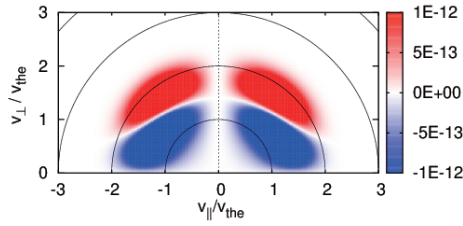


Fig. 1 The quasi-linear diffusion term of ECH.

linear effect, $S^{\text{ql}}(\delta f)$, in the quasi-linear diffusion source term for simplicity. Since we evaluate the force by ECH in the steady state, we assume that the density and the temperature are constant. Under these conditions, the source term S^{ql} is given by [9]

$$S^{\text{ql}}(f_{\text{Max}}) = -\delta(\vec{r} - \vec{r}_0) \cdot \frac{\partial}{\partial v_i} D_{ij}^{\text{ql}} \frac{\partial f_{\text{Max}}}{\partial v_j}, \quad (2)$$

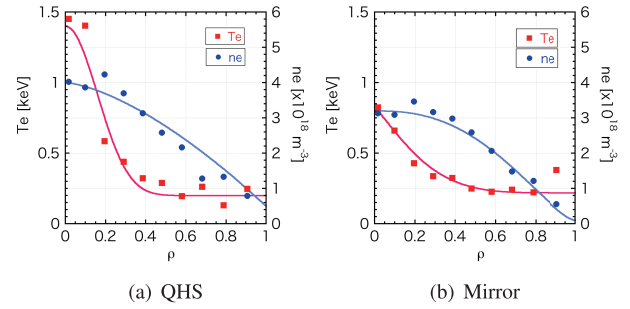
where D_{ij}^{ql} is the quasi-linear diffusion tensor, and \vec{r}_0 is the heating position obtained by the ray-tracing code. We use the ECH deposition profile as the distribution in the real space, instead of the delta function. The fundamental O-mode ECH is applied in HSX. One typical case of the quasi-linear source term is shown in Fig. 1, which shows the heating from the blue region to the red one.

ECH can drive the radial electron current j_e . The net current in the steady state should vanish to maintain the quasi-neutrality, so the return current, $j_r (= -j_e)$, must flow in the bulk plasma except for energetic electrons generated by ECH. Therefore, the bulk plasma feels $j_r \times B$ force due to the return current.

On the other hand, the supra-thermal electrons drift toroidally due to the precession motion. During the slowing down of the supra-thermal electrons, they transfer their momentum to the bulk plasma due to collisions. If we consider the isotropic source, the force of the passing particles in the Co direction cancels that of the passing particles in the Counter direction. The trapped particles, however, have a precession motion, which can contribute to the net collisional force. The two forces should cancel in the completely symmetric configuration in the symmetry direction [10]. Therefore, the total toroidal force should vanish in the axisymmetric configuration. However, non-symmetric magnetic modes enhance the radial electron flux and break the cancellation of the two forces.

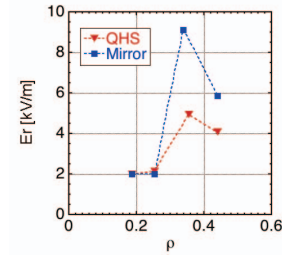
3. Simulation Results

We performed the simulations assuming typical experimental conditions regarding the temperature, density, and radial electric field of HSX plasma as shown in Fig. 2. The temperature and density were fitted and the radial electric field was interpolated in the simulations. The plasma parameters were as follows: magnetic axis major radius $R_{\text{ax}} \sim 1.2$ m; averaged minor radius $a \sim 0.15$ m; toroidal magnetic field strength $B_T = 1.0$ T; and ECH power P_{ECH}



(a) QHS

(b) Mirror



(c) The radial electric field

Fig. 2 (a) and (b): The experimental data of the density and the electron temperature. (c): The measured radial electric field in both experiments. The plots are experimental data, and the lines are fitting of them. In simulations, the fitting profiles are used.

$= 100$ kW. In HSX experiments, the absorption power was about 30 kW, and the absorption rate depended on the density and the temperature. Now, we set the ECH power at 100 kW in all the simulations to focus on the configuration difference. We used the magnetic configurations calculated in the low- β limit as the QHS and Mirror configuration. Also, we used the (0,0) and (0,4) modes of the QHS configuration as the completely helically symmetric configuration.

Applying GNET code, we evaluated the velocity distribution of δf in the QHS configuration. Figures 3(a) and 3(b) show the velocity distribution at normalized minor radius $\rho \sim 0.1$ and 0.3 surface. The velocity distribution integrated over the volume, total δf , is shown in Fig. 3(c). They show deviation from the Maxwellian distribution, where the red region means increasing and the blue region decreasing. Energetic electrons can be found in the outer regions apart from the heating point, which indicates that there is a radial electron flux, as shown in Fig. 4. Since we are not concerned about the local distribution, we integrate the velocity distribution over the flux surface and treat it in the term of a minor radius.

HSX has the helical symmetry of the (1,4) mode, so we have to consider a two-dimensional force, as shown in Fig. 5. Here, we evaluate the helical force, that is, the helical component of the force. We cannot compare the sizes of the vectors among the three configuration in Fig. 5 because it has been emphasized to make it easy to understand. Also, we use the toroidal-poloidal angle as the axis, not θ

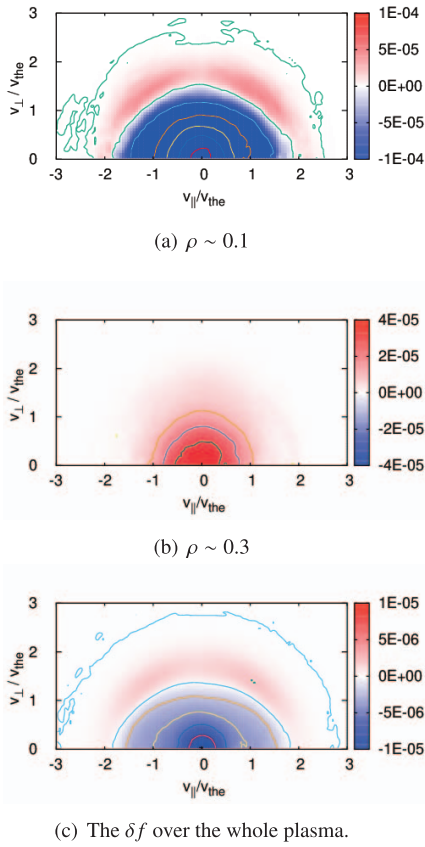


Fig. 3 The velocity distribution function, δf with contour lines. They show the deviation from Maxwellian.

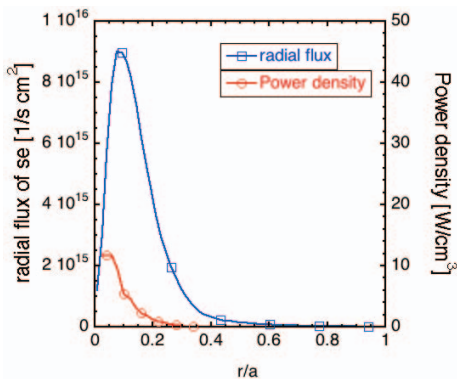


Fig. 4 The radial flux profile of supra-thermal electrons and the absorption power density.

and $R\phi$, for simplicity. As a result, the total force in the completely symmetric configuration is almost perpendicular to the symmetry direction. However, even in the QHS configuration, the $j_r \times B$ force is much larger than the collisional force, and the total force has the component parallel to the helically symmetry direction. The direction of the parallel component is the same as that of the flow observed in the experiments [11]. We consider that the symmetric component is important for the flow.

Figure 6 shows the helical force in each configuration.

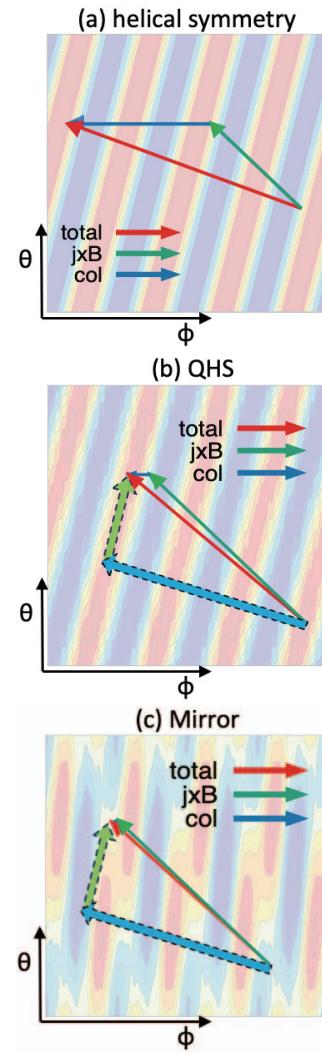


Fig. 5 The direction of each force. (a) shows that of the completely helically symmetric configuration, (b) shows that of QHS configuration, and (c) shows that of Mirror configuration. The green dashed vector is the component of helical symmetry direction, and the blue dashed vector is its perpendicular component. The background contour shows the magnetic field strength pattern.

In the completely helically symmetric configuration, the total force is quite small. Even the QHS configuration has a net force of the symmetry direction. As noted above, the $j_r \times B$ force is dominant in the QHS and Mirror configurations. Also, the force in Mirror configuration is almost three times larger than that in the QHS configuration. The magnitude relationship of the forces is consistent with that of the experimental flow velocity. We have to consider the viscosity, which modifies the flow velocity, for a more precise flow prediction.

To investigate the differences in the helical force and radial orbit among these configurations, we calculated the collisionless drift orbit of the energetic electrons with energy $E = 5$ keV and pitch angle $\lambda \sim 20^\circ$ (passing) or 80° (trapped). The orbits for each configuration are shown in

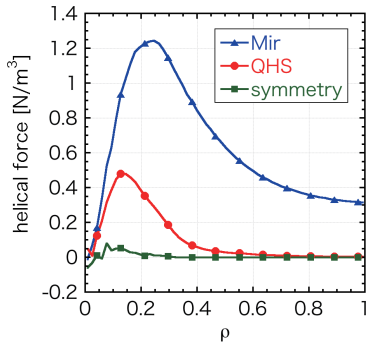


Fig. 6 The helical total force. They include $j_r \times B$ and collisional force.

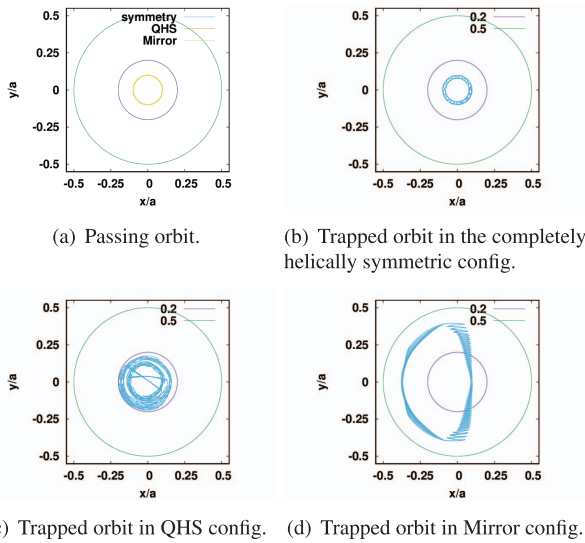


Fig. 7 The collisionless orbit of a supra-thermal electron. Fig. (a) shows the passing orbits of the three configurations and Figs. (b) - (d) shows each trapped orbit.

Fig. 7. As seen in Fig. 7 (a), the orbits of passing particles are the same among the three configurations, so the three orbits look like one line. However this is not the case for the trapped particle. In the completely symmetric configuration, the helically trapped particle goes around and does not move radially. To the contrary, the particle goes radially in the QHS configuration. The orbit in the Mirror configuration is much larger than that in the QHS configuration.

The radial flux can be roughly understood as the radial mean free path, which is determined by the collision frequency and the radial drift velocity. When the collisionality is low enough for electrons to move along the drift orbit, a larger orbit produces more flux. Differences in the magnetic configurations cause differences in the electron radial flux through the orbits. Therefore, the $j_r \times B$ force is much smaller in the completely helically symmetric configuration, and the force in the Mirror configuration is larger than that in the QHS configuration.

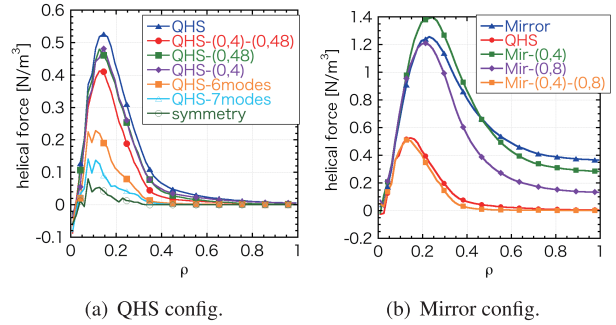


Fig. 8 Helical force profiles not including several modes: (a) and (b). (a) The blue line includes the full QHS magnetic modes and the green bottom line with open circles only includes the (0,0) and (1,4) mode. The other lines do not include several modes. (b) The blue line includes the full Mirror magnetic modes and red line is the same as the case of the full QHS modes. The others do not include the (0,4) and/or (0,48) modes.

The QHS configuration does not only have a helically symmetric mode but also other non-symmetric modes. Additionally, the Mirror configuration has two large non-symmetric magnetic modes. The effect of non-symmetric modes is shown in Fig. 8. In the QHS configuration, the strength of seven non-symmetric mode spectrum is 10 ~ 20% of (1,4) mode near the axis ($\rho \sim 0.1$). They enhance the radial flux as seen in Fig. 8. The strength of the helical force corresponds to the radial flux because the $j_r \times B$ force is dominant in the helical force. If we ignore each magnetic mode one by one, the helical force decreases slowly. If none of the seven modes are included, the profile is similar to that of the helical symmetry case. Therefore we can consider that the seven non-symmetric modes affect the radial flux and $j_r \times B$, although there is no especially dominant effective mode among them. In the Mirror configuration, the Mirror terms, that is, the (0,4) and (0,8) mode, dominate the enhancement of the radial flux. Since the Mirror terms are strong non-symmetric modes, they change the electron orbits drastically and enhance the electron flux. Except for the two Mirror terms, the magnetic configuration is similar to the QHS configuration, and the helical force has a very similar profile to that of the QHS case.

4. Conclusions

We have evaluated the collisional and $j_r \times B$ forces caused by ECH, using GNET code. In the helically symmetric configuration, the collisional and $j_r \times B$ forces almost cancel each other in the direction of symmetry. The QHS and Mirror configurations have a component in the symmetry direction. Experimentally, the plasma flows in the symmetry direction while the flow in the direction perpendicular to the symmetry quickly damps. Therefore, we consider that the helical force is important. As a result, we obtained a larger force in the Mirror configuration than in the QHS configuration. The magnitude relationship of

the forces is consistent with that of the experimental flow velocity. It was also found that what makes the difference among the three configurations is the radial orbit modified by the non-symmetric magnetic modes. The radial drift consequently enhances the radial flux and the $j_r \times B$ force. Here, the $j_r \times B$ force is much larger than the collisional force in the non-symmetric configuration.

To compare the simulations with the experiments, we must solve the momentum balance equations with viscosity and force. Now we are tackling the flow calculation. In the neoclassical prediction, the flow should be small in the core region where the gradients are small. However a large flow was observed in the Mirror configuration. As a preliminary calculation, we solved the momentum balance equations with some limitations and assumptions. The $j_r \times B$ force makes the parallel flow to the magnetic field line in the expected direction. Therefore, the force produced by ECH would explain the large flow in the Mirror configuration.

The authors would like to thank HSX group for providing data and fruitful discussions. This work is sup-

ported by a Grant-in-Aid for Scientific Research (C), No. 18K03582, and The Kyoto University Foundation. This work was carried out using the Plasma Simulator (FUJITSU FX100) of NIFS and JFRS-1 supercomputer system at IFERC-CSC.

- [1] M. Yoshida *et al.*, Nucl. Fusion **49**, 115028 (2009).
- [2] P.H. Diamond *et al.*, Nucl. Fusion **53**, 104019 (2013).
- [3] A.F. Almagri *et al.*, IEEE Trans. Plasma Sci. **27**, 114 (1999).
- [4] J.M. Canik *et al.*, Phys. Plasmas **14**, 056107 (2007).
- [5] A. Briesemeister *et al.*, Plasma Phys. Control. Fusion **55**, 014002 (2013).
- [6] S.T.A. Kumar *et al.*, Plasma Phys. Control. Fusion **60**, 054012 (2018).
- [7] T.J. Dobbins *et al.*, Nucl. Fusion **59**, 046007 (2019).
- [8] S. Murakami *et al.*, Nucl. Fusion **40**, 693 (2000).
- [9] M. Brambilla, *Kinetic Theory of Plasma Waves Homogeneous Plasmas* (Oxford Science Publications, 1998).
- [10] M.N. Rosenbluth and F.L. Hinton, Nucl. Fusion **36**, 55 (1996).
- [11] A. Briesemeister *et al.*, Contrib. Plasma Phys. **50**, 741 (2010).